Journal of Power Sources 197 (2012) 161–167

Contents lists available at SciVerse ScienceDirect

Journal of Power Sources

journal homepage: www.elsevier.com/locate/jpowsour

A synchronous investigation of the degradation of metallic bipolar plates in real and simulated environments of polymer electrolyte membrane fuel cells

Yann-Cheng Chen [a], Kung-Hsu Hou [b], Chien-Hung Lin [c], Ching-Yuan Bai [b], Nen-Wen Pu [d], Ming-Der Ger [a,*]

[a] Department of Chemical and Materials Engineering, Chung Cheng Institute of Technology, National Defense University, Tau-Yuan 335, Taiwan, ROC
[b] Department of Power Vehicles and System Engineering, Chung Cheng Institute of Technology, National Defense University, Tao-Yuan 335, Taiwan, ROC
[c] School of Defense Science, Chung Cheng Institute of Technology, National Defense University, Tao-Yuan 335, Taiwan, ROC
[d] Department of Photonics Engineering, Yuan Ze University, Chung-Li, Tao-Yuan 320, Taiwan, ROC

ARTICLE INFO

Article history:
Received 2 September 2011
Accepted 14 September 2011
Available online 19 September 2011

Keywords:
Metallic bipolar plates
Degradation
Ohmic resistance
Potentiodynamic polarization
Interfacial contact resistance

ABSTRACT

We propose a method to investigate the degradation of metallic bipolar plates (BPPs) synchronously in real and simulated environments of PEM fuel cells. In order to eliminate the uncertainty factor of cell performance resulting from the degradation of the polymer membrane, a simulated PEMFC environment separated from the cell system was created, and the results from real and simulated environments can be directly compared. All of the BPPs aged in real operation and in a simulated environment are used to assemble single cells with the same fabricating and activating conditions. Based on the fitting results for the polarization curves of single cells, the cell ohmic resistance (R) shows a tendency to linearly increase with time, and the increasing rate in the simulated environment is higher than that in real operation. Moreover, the surface morphologies and corrosion behaviors of the BPPs having undergone real or simulated tests are examined. The results indicate that the simulated environment causes more severe degradation of BPPs than the real situation. Therefore, the temporal evolution in the surface conductivity of BPPs is also explored, to evaluate the effect of interfacial contact resistance on the degradation of cell performance. This study can provide a reference method for the preliminary evaluation and design of metallic BPPs.

1. Introduction

The urgent problems of global warming and fossil fuel exhaustion have been the most important world energy issues in the past decades. The demand for energy is increasing dramatically with industrial development and is causing an energy revolution by requiring alternative energy sources and changes in lifestyle. Because of the desirable characteristics of polymer electrolyte membrane fuel cells (PEMFCs), such as high energy conversion efficiency, very low chemical and acoustical pollution rates, and remarkable performance in the application of vehicle power, these materials are expected to play a major role in energy systems in industry and in our daily lives for the foreseeable future. In the performance studies of fuel cell operation, most of the previous research has focused on the degradation of membrane electrode assemblies (MEAs) [1–5]. However, bipolar plates (BPPs) as a multifunctional component with great influence on cell performance are also one of the most important parts in PEMFCs. Conventionally, graphite bipolar plates have accounted for approximately 80% of the total weight and 45% of the stack cost, which is one of the major troubles for the commercialization of PEMFCs. Metallic materials have been considered an alternative to graphite because of their malleability and superior mechanical properties, allowing designs of a smaller and thinner stack to reduce the weight and volume of fuel cells [6–11]. The main challenge for metal BPPs is that passive oxides, which would develop on the surfaces and protect metals against the progression of corrosion, cause the undesirable effects of raising the surface contact resistance and reducing the cell performance [7–10]. In addition, metal BPPs were prone to dissolution in an acidic (pH 2–3) and humid environment at temperatures around 80 °C (the PEMFC system environment). The dissolved metal ions may poison the MEA and deteriorate

* Corresponding author at: Electrochemical Microfabrication Lab, Department of Chemical and Materials Engineering, Chung Cheng Institute of Technology, National Defense University, Ta-His, Tao-Yuan 335, Taiwan, ROC. Tel.: +886 3 3891716; fax: +886 3 3892494.
E-mail address: mingderger@gmail.com (M.-D. Ger).

0378-7753/$ – see front matter © 2011 Elsevier B.V. All rights reserved.
doi:10.1016/j.jpowsour.2011.09.032

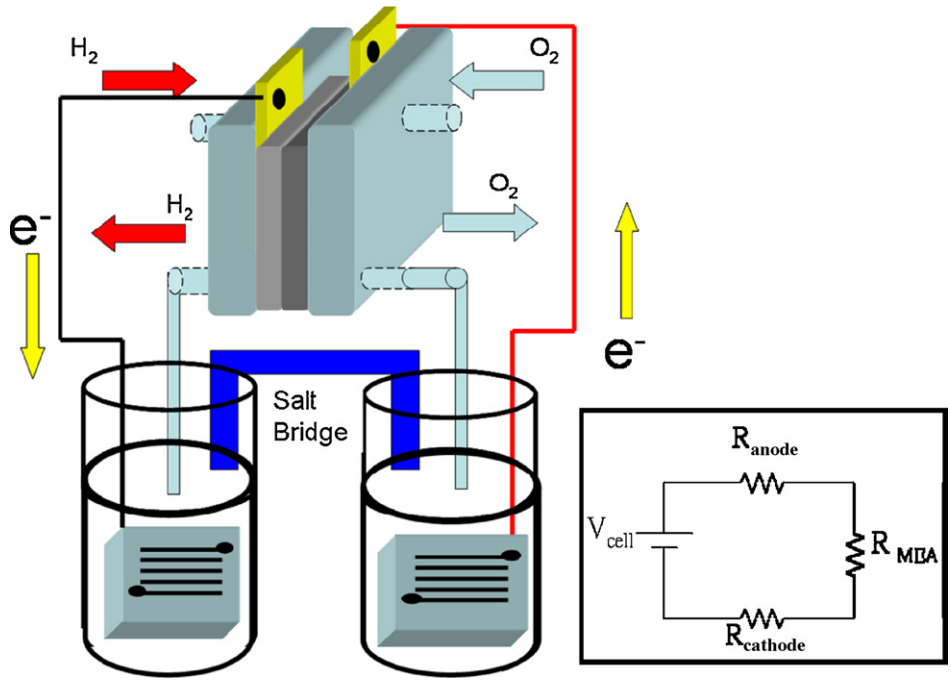

Fig. 1. A schematic diagram of the experimental apparatus and its equivalent circuit.

the performance of fuel cells. It is essential to understand the degradation phenomena for metallic BPPs in real and simulated environments in order to modify their characteristics and elevate the durability and lifetime of PEM fuel cells. Therefore, this work expands an investigation method for studying the performance degradation of metallic BPPs synchronously in real and simulated environments.

Thus far, many experiments on the performance of metallic BPPs using in situ and ex situ methods have been carried out and published [12–17]. For in situ test methods, Makkus et al. performed a long-term durability test (approximately 7000 h) and measured the change of the interfacial contact resistance between BPPs and gas diffusion layers (GDLs) [12]. The method has been extensively adopted as an in situ technique to evaluate the performance of metallic BPPs. Hodgson et al. executed a long-term (8000 h) performance test of a single cell fabricated with special metallic BPPs, which were coated with FC5 materials produced by the ICI Company [13]. Moreover, Wind et al. analyzed the amounts of metal ions dissolved from the metallic BPPs and contaminating the MEA surface to evaluate the durability of metallic BPPs [14]. For ex situ test methods, Wang et al. suggested a simulated PEMFC environment with a solution of 1 M H_2SO_4 + 2 ppm HF at 70 °C, bubbled with hydrogen on the anode and oxygen on the cathode [15]. The experiment was performed on four stainless steel specimens to investigate their corrosion resistance and interfacial contact resistance. Also, Lafront et al. carried out a similar ex situ experiment on stainless steel and $Zr_{75}Ti_{25}$ alloys using an electrochemical noise test after immersing the metallic BPPs in a simulated PEMFC environment (12.5 ppm H_2SO_4 + 2 ppm HF at 80 °C) for 3 h [16]. Additionally, Wang et al. operated the corrosion test of BPPs in a simulated PEMFC environment (0.5 M sulfuric acid solution) at 20 °C for 5000 h, and then performed the ex situ experiment using the open-circuit potential, AC impedance, and inductively coupled plasma optical emission spectrometry (ICP-OES) to analyze the corrosion resistance and amounts of metal ions dissolved from metallic BPPs [17].

As described above, the performance of metallic bipolar plates is usually examined in a real cell operation (in situ) or in a simulated environment (ex situ) independently, and most of the published research focuses on the surface corrosive behaviors and the ultimate conditions of metallic BPPs. Until now, there has been no literature published that synchronously investigated and discussed the relationship between the degradation of metallic BPPs in real and simulated environments. For this reason, we made the effort to design a testing apparatus that correlates the simulated environments with an operational PEMFC. This technique offers three advantages to the conventional experiment. First, the metallic BPPs in the simulated environment were separated from the real cell operation to avoid the

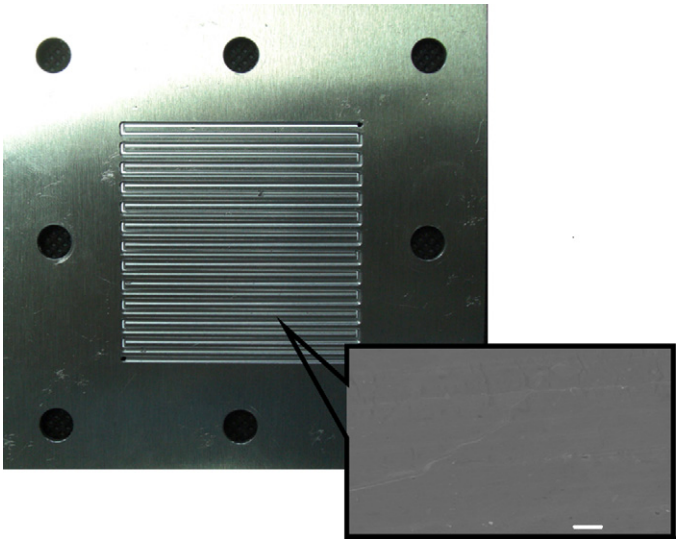

Fig. 2. An Al-alloy bipolar plate with a flow-field pattern and the SEM topography at the bottom of flow field.

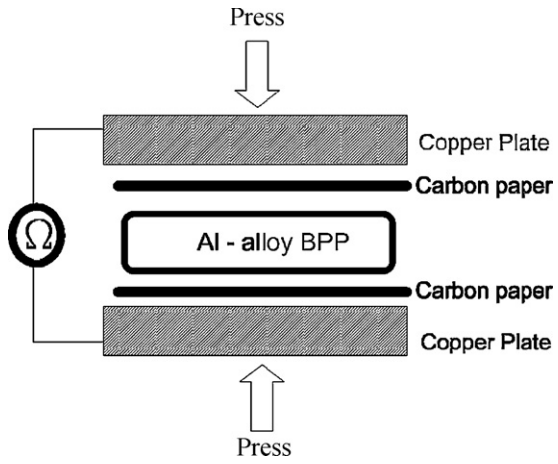

Fig. 3. The measurement setup for interfacial contact resistance.

interaction between the BPPs and the membrane. Hence, the uncertainty in the amount of performance degradation that is attributable to the polymer membrane or to the metallic BPPs can be eliminated. Secondly, the simulated environment was operated synchronously with the real PEMFC. The temporal variation of the BPP's surface could be investigated without taking the PEMFC apart. Finally, these specimens in the simulated environment can easily be examined at any aging time, using various instruments.

The degradation of BPPs could be explored in a shorter amount of time by running the simulated and real-cell tests synchronously, and the experimental results would be more precise than those of conventional simulation methods. Moreover, this synchronous testing method can be employed extensively for the degradation investigation of many metallic BPPs, although only Al-alloy 5052 was used as the example material for the BPPs in this study.

2. Experiments

2.1. Experimental setup and components

The schematic diagram of this experimental apparatus and its equivalent circuit, which connected the simulated environment with a real operation PEMFC, are shown in Fig. 1. The total resistance is composed of R_{anode}, $R_{cathode}$, and R_{MEA}.

For this electric circuit, the resistance can be expressed as

$$R_{total} = R_{anode} + R_{cathode} + R_{MEA} \quad (1)$$

where R_{anode} and $R_{cathode}$ are the resistances, including the intrinsic resistance of BPPs and the contact resistance between BPP and MEA at the anode and cathode, respectively. The MEA is considered a whole unit in the fuel cell, and R_{MEA} is its resistance under the real PEMFC operation. The resistance of the proton exchange membrane is an uncertain parameter within the PEMFC because of the performance reduction factors for membrane degradation and the poisonous behavior of metal ions dissolved from metallic BPPs. Moreover, the main degradation factors attributed to BPPs or the proton exchange membrane are not easy to identify. Therefore, a whole resistance unit, R_{MEA}, is adopted to substitute for the membrane or electrolyte resistance in the equivalent circuit.

The single PEMFC in this study was manufactured with a commercial membrane electrode assembly (MEA), machined 5052 Al-alloy BPPs, and gas diffusion layers. The MEA consisted of

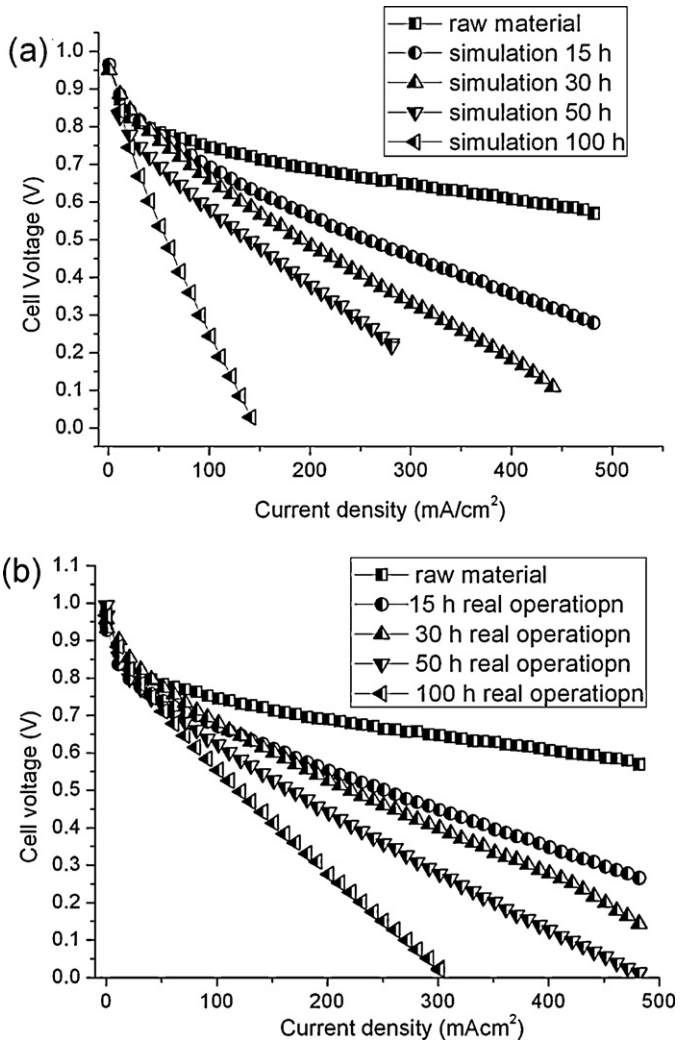

Fig. 4. The *I–V* curves of single cells assembled with the Al-alloy BPPs having undergone (a) simulated testing and (b) real operation.

Table 1
The fitting parameters for the *I–V* curves of 5052 Al-alloy BPPs aged under various experiment conditions.

Specimens (BPPs)	Aging time (h)	E_0 (V)	b (V dec^{-1})	R (Ω cm^2)	m (mV)	n (cm^2 mA^{-1})	Root mean square error
Raw materials	–	0.806	0.032	0.013	0.0025	0.0511	0.009
Under real operation	15	0.78	0.027	0.027	0.055	0.035	0.0008
	30	0.827	0.023	0.052	0.010	0.042	0.017
	50	0.78	0.031	0.070	0.029	0.1367	0.007
	100	0.81	0.023	0.107	0.040	0.055	0.0019
Under simulated environment	15	0.872	0.029	0.038	0.0517	0.026	0.018
	30	0.831	0.025	0.061	0.0084	0.0502	0.001
	50	0.825	0.027	0.079	0.00308	0.019	0.008
	100	0.845	0.032	0.232	0.007	0.018	0.017

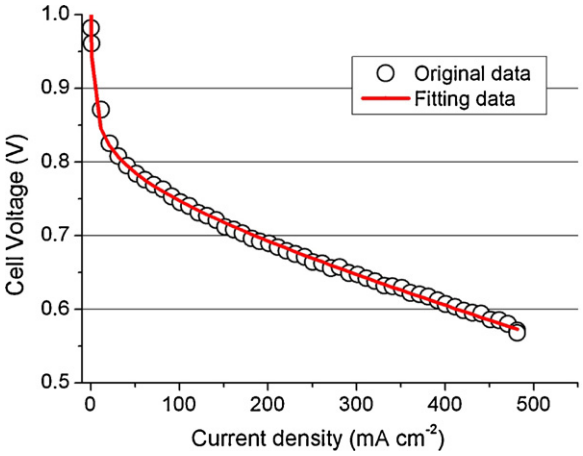

Fig. 5. Fitting of the original polarization curve for the single cell with raw Al-alloy BPPs.

Nafion 112 membranes and Toray paper with a catalyst loading of 0.2 mg cm^{-2} on the anode and 0.4 mg cm^{-2} on the cathode electrode. An Al-alloy BPP, machined with single serpentine flow-field with an active area of 25 cm^2 is shown in Fig. 2, and the SEM topography at the bottom of the flow-field in the BPP was inserted in this figure.

While the single cell mentioned above was operated, the reaction gases were introduced to the cell, and the hydrogen gas was oxidized to H^+ ions and electrons at the anode side. The reaction at the negative electrode is given by

$$2H_2 \rightarrow 4H^+ + 4e^- \quad (2)$$

Moreover, hydrogen ions were transported to the cathode side and reacted with the oxygen gas. The reaction at the positive electrode is given by

$$O_2 + 4e^- + 4H^+ \rightarrow 2H_2O \quad (3)$$

The liquid produced by the electrochemical reaction in the single cell and the excessive reaction gases were introduced into the beakers, which contained the basic solution for the simulated environment.

The solution in the beakers was mixed with 12.5 ppm sulfuric acid and initially set at approximately pH 6.5. Specimens of the Al-alloy BPPs were immersed in the solution with bubbling hydrogen at the anode side (104 sccm) and oxygen at the cathode side (70 sccm). The simulated solutions in the beakers and the real fuel cell were controlled at the same temperature of 343 K. Moreover, the electrodes of bipolar plates were connected to the collectors of the single cell using electrical wires. The electrons can drift from the anode side to the cathode side, and the reduction reaction of oxygen occurs while the electric charges are transported via the external circuit and the salt bridge. Based on the experimental setup, this novel method takes into account the mass transport effects, which differs from conventional methods.

2.2. Assembly (single cell) tests and surface characterization of bipolar plates

All of the bipolar plates aged in both real operation and in a simulated environment for 15, 30, 50, and 100 h are used to assemble the single cells with the same fabricating and activating conditions. A compaction force of 200 N was evenly loaded on every bolt to assemble the components of the single PEM cell. Prior to the cell operation, nitrogen was used to purge the cell of residual gases. The as-built single cells were operated at 343 K under ambient pressure. Pure hydrogen and oxygen were used as reactant gases

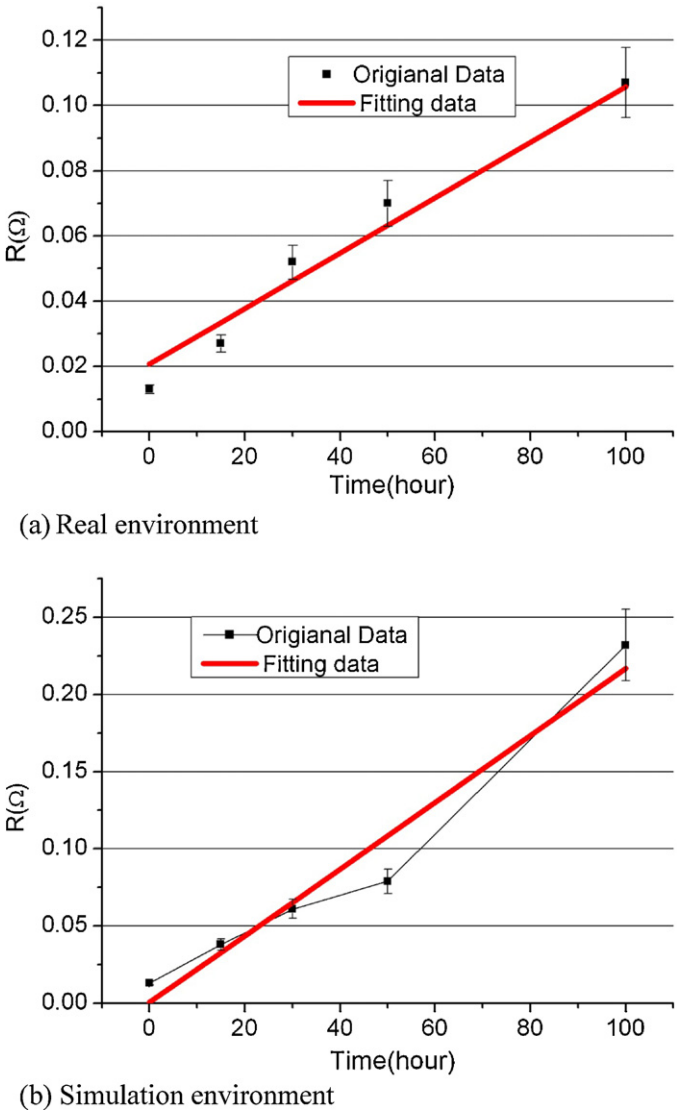

Fig. 6. Values of ohmic resistance, derived from the fitting model for (a) real and (b) simulated conditions, as a function of BPP aging time.

at the anode and cathode sides with the flow rates of 104 sccm and 70 sccm, respectively. Moreover, cell voltages as a function of current density for the tested single cells were measured in the operation region, and then the recorded curves were fitted with a suitable mathematical model.

In addition, the surface morphologies and compositions of the bipolar plates, aged in real operation and a simulated environment for various amounts of time, were examined using scanning electron microscopy (SEM) with X-ray energy dispersive spectrometry (EDS).

2.3. Electrochemical test

Potentiodynamic polarization was employed to analyze the corrosion resistance of Al-alloy BPPs precorroded (aging) in real operation and a simulated environment for 15, 30, 50 and 100 h (aging time). The tests implemented an Autolab electrochemical interface, and the data were analyzed with Geps software. A saturated calomel electrode (SCE) was used as a reference to measure the potential across the electrochemical interface. The tests were carried out by sweeping a potential range from −0.8 V to −0.1 V

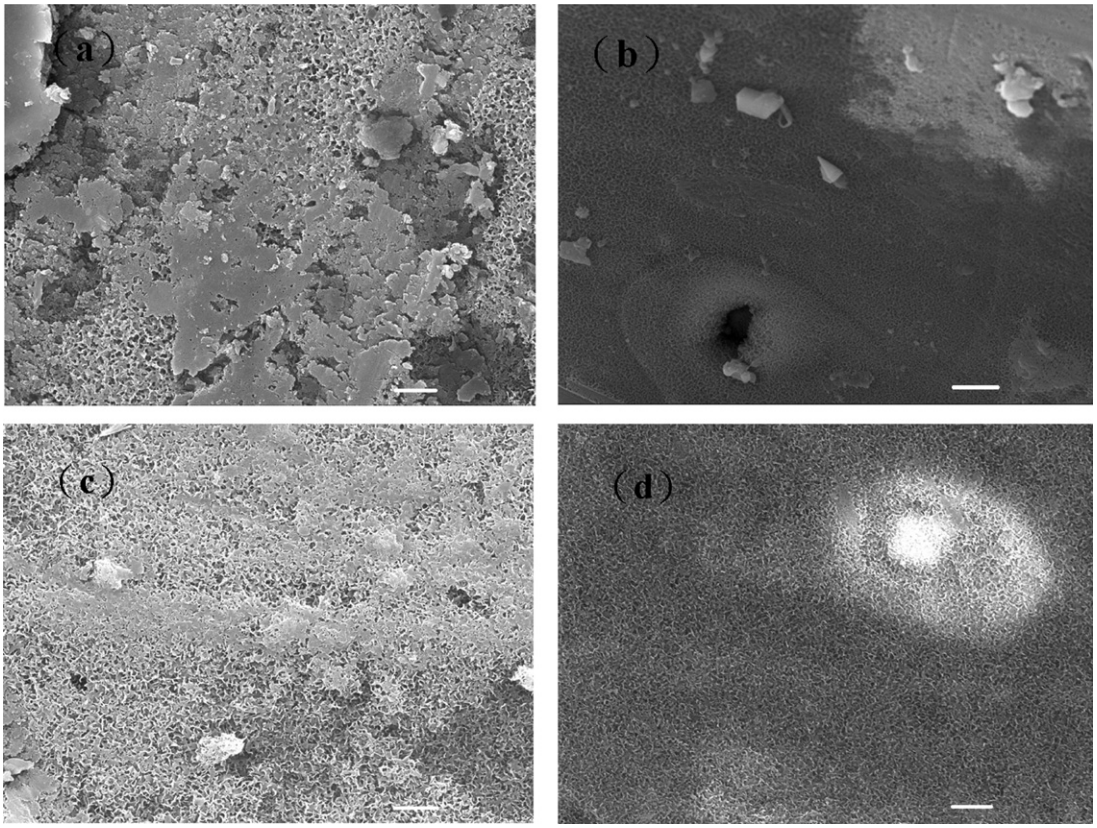

Fig. 7. SEM surface micrographs of the BPPs operated under the experimental setup for 50 h: (a) cathode side in the real condition; (b) anode side in the real condition; (c) cathode side in the simulated environment; (d) anode side in the simulated environment.

with a scanning rate of 0.5 mV s^{-1} in a 0.5 M H_2SO_4 solution without purging any gases at room temperature.

2.4. Interfacial contact resistance (ICR) measurement

The measurement method for interfacial contact resistance between the Al-alloy BPPs and GDL is illustrated in Fig. 3, which is similar to previous studies [18]. The measured total resistance (R_{T1}) is composed of the resistances of Al BPPs (R_{Al}), two GDLs ($2R_{GDL}$), two copper plates ($2R_{Cu}$), and four interfacial components—two bipolar plate/carbon paper ($2R_{GDL/Al}$) and two carbon paper/copper plate ($2R_{Cu/GDL}$) interfaces. R_{T1} is expressed as follows:

$$R_{T1} = 2R_{Cu} + 2R_{Cu/GDL} + 2R_{GDL} + 2R_{GDL/Al} + R_{Al} \quad (4)$$

Eq. (5) gives the resistance (R_{T2}) when one carbon paper is placed between two copper plates without bipolar plates. The resistance of the GDLs could be neglected because the bulk resistance of GDLs is very small, and then the interfacial contact resistance between bipolar plate and GDL can be calculated by subtracting those values from the total resistance (R_{T1}) measured with the metal bipolar plate in place (listed in Eq. (6)).

$$R_{T2} = 2R_{Cu} + 2R_{Cu/GDL} + R_{GDL} \quad (5)$$

$$2R_{GDL/Al} = R_{T1} - R_{T2} - R_{Al} \quad (6)$$

3. Results and discussion

The performance of single cells that were assembled with both of the BPPs aged in real or simulated environments for 15, 30, 50 and 100 h, was tested using the polarization (open circuit voltage vs. current) technique, and the difference in cell performance between the BPPs undergoing real or simulated operation was also investigated in this study. Moreover, the change of the BPP's characteristics with time was studied by microstructure observation, electrochemical polarization, and interfacial contact resistance tests. The results and accomplishment of this technique are described and discussed as follows.

3.1. Cell performance and mathematical fitting

Fig. 4(a) and (b) shows the *I–V* curves of single cells assembled with the Al-alloy BPPs having undergone simulated testing and real operation, respectively, for various aging times. As presented in Fig. 4, the open circuit voltages (OCV) or performance of all of the single cells at a low current density are almost equivalent, but the voltage decreases with increasing current density. The results also show that the cell performance dropped with increasing aging time under both real and simulated conditions. The degradation of cell performance mainly resulted from the corrosion phenomenon and the formation of passive oxides on the surface of BPPs. Oxide films developed on the surfaces would decrease the efficiency of mass and electron transport and raise the contact resistance between the BPP and the GDL. Thus, the cell performance would drop with increasing aging time as a result of oxide film thickening [19]. Moreover, the *I–V* curve slope for 30 h in a simulated environment, shown in Fig. 4(a), approximately matches that for 50 h of real operation, shown in Fig. 4(b). This result indicated that the simulated PEMFC environment was more stringent than the real operation condition, and this experimental method can be utilized for accelerated aging (test) of metallic BPPs.

Kim et al. developed a mathematical model for polarization (*I–V*) curves in PEMFCs with an empirical equation [20], given here in

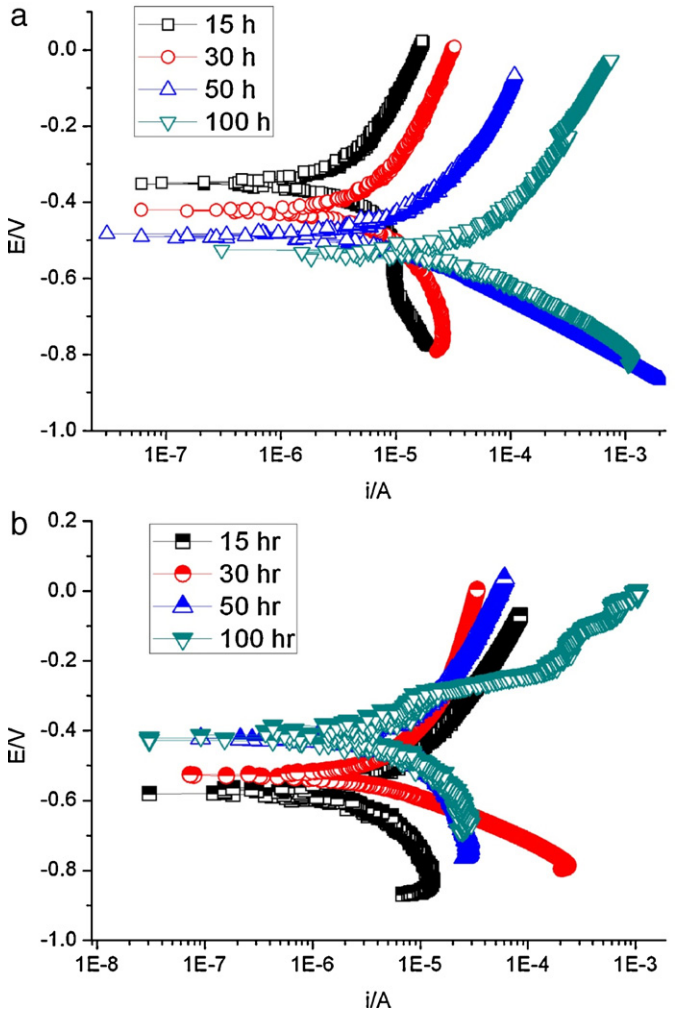

Fig. 8. Polarization curves of the Al alloy BPPs aged in simulated (a) anode or (b) cathode environments for various times, measured in a 0.5 M H_2SO_4 solution.

Eq. (7), to point out the relationship between the single cell performances and various parameters:

$$E = E_o - b\log(i) - Ri - m\ \exp(ni) \quad (7)$$

The term E_o is an electrode kinetic parameter, b is the Tafel parameter, and R represents the ohmic resistance that causes a linear variation of E with i. The values of m and n depend on the physicochemical parameters of the system, such as temperature and pressure. The final term on the right side of Eq. (7) takes the mass transfer effect into consideration.

The initial I–V curve for the single cell assembled with raw Al-alloy BPPs was fitted using this equation. The original data and fitting curve are shown in Fig. 5, in which the root-mean-square error was approximately 0.009, indicating that the fitting result is good and the data do follow the mathematical model. Moreover, the polarization curves of the cells assembled with aged Al-alloy BPPs were also fitted, and the fitting parameters for every curve are listed in Table 1.

The values of ohmic resistance (R) derived from the fitting model for real and simulated conditions as a function of the BPP's aging time are plotted in Fig. 6. As shown in the figure, the R values increase linearly with increasing aging time under both real and simulated conditions. Therefore, it can be confirmed with this mathematical model that the degradation tendency of the BPPs operated in a real cell is similar to that in the simulated PEMFC environment.

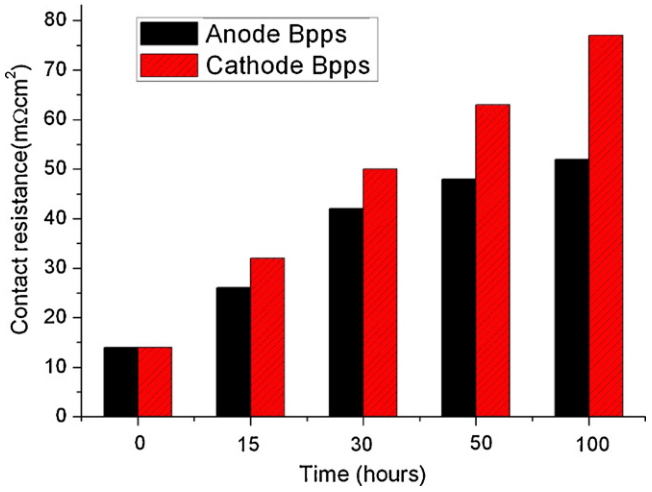

Fig. 9. The ICRs of anode and cathode BPPs measured at the compaction pressure of 200 N cm^{-2}.

3.2. Corrosive behaviors of the metallic bipolar plates

The Al-alloy BPPs exposed to real or simulated environments were used to assemble single cells. After cell performance tests, the corrosive behaviors of the Al-alloy BPPs were examined using SEM with EDS analyses. The SEM surface micrographs of the tested bipolar plates, which were precorroded (aged) in real or simulated conditions for 50 h, are shown in Fig. 7. As seen in Fig. 7(a) and (c), large amounts of oxides developed on the cathode side of the bipolar plates. In fact, the thickness of these oxide films increased with increasing aging time owing to the high oxygen concentration in the cathode condition. In contrast, the morphologies of the dissolving surface were observed in Fig. 7(b) and (d), indicating that oxide films could not easily form on the anode side of the bipolar plates where hydrogen flows in and oxygen is lacking. The results of EDS analyses on the BPP surface revealed that the oxygen concentration on the cathode side (54.5 at%) was much higher than that on the anode side (10.78 at%). It was verified that the acid electrolyte in typical PEM fuel cell atmospheres results in seriously corrosive behavior, and a passive layer with large amounts of oxides easily forms on the cathode surface of Al-alloy BPPs.

PEM fuel cells usually operate in the temperature range of 70–100 °C to reach good performance. However, significant amounts of metallic ions would be dissolved from BPPs and contaminate the proton exchange membranes while the cells operate in this condition. Hence, the concentration of metal ions in fuel cells is an important indicator to evaluate the performance of metallic BPPs [17]. In order to estimate the contamination effect of the Al ions dissociated from the Al-alloy BPP, the concentration of Al ions in the simulated (beaker) solution was measured using ICP-MS after 50 h operation under the experimental setup. The concentrations of Al ions produced at the cathode and anode sides were approximately 1.5 ppm and 35.2 ppm, respectively. The aluminum ion concentration in the anode solution is higher than in the cathode solution, indicating that the anode environment is more severe than the cathode side. The ICP analysis is consistent with the results of SEM with EDS. Therefore, surface modification of Al alloy BPPs is needed to improve the performance of PEMFCs.

3.3. Corrosion resistance test

Fig. 8 shows the potentiodynamic polarization curves of the Al-alloy BPPs, which were aged in simulated anode and cathode environments for 15, 30, 50, and 100 h. The corrosion current density of the Al alloy BPPs aged on the simulated anode side

(where hydrogen enters) is much larger than that on the cathode side (where oxygen enters) for various aging times. Obviously, the results of the corrosion resistance test agree with the observation and analyses of the BPP's surface made with SEM. In other words, the Al-alloy BPPs aged in the simulated cathode environment showed better corrosion resistance than those aged in the anode environment. This finding is attributed to the formation of an oxide layer on the surface of cathode BPPs, which reduces the corrosion rate because of the high oxygen concentration in the cathode environment during the aging treatment. However, the corrosion current density of Al alloy BPPs increased with increasing aging time for both the anode and cathode. It is indicated that the oxide layer that formed on the cathode BPPs was continuously corroded or dissolved in the acidic electrolyte, and therefore, the anticorrosive performance of cathode BPPs would decline with increasing aging time.

3.4. Interfacial contact resistance (ICR)

The interfacial contact resistance between the Al-alloy BPPs and GDLs was measured under various compaction pressures, in which the BPPs were aged in the simulated anode or cathode environments for 0, 15, 30, 50, and 100 h. In this experiment, the total resistance contains four interfacial components and the resistances of bulk materials, as mentioned in Section 2.4 [18]. Both the total resistance and ICR values, measured in various aged Al-alloy BPPs, decrease noticeably with increasing compaction pressures when the compaction pressure is lower than 50 N cm^{-2}. At the pressure range of 50–100 N cm^{-2}, the ICR values decrease moderately with increasing compaction pressure. When the compaction pressure is higher than 100 N cm^{-2}, the change of contact resistance with compaction pressure becomes smoother. It is assumed that the electric current flowing through the interfaces between the assembled components of fuel cells would increase with increasing compaction force as a result of enlarging contact areas of all components, and therefore, the total resistance and contact resistances of all interfaces would decrease with increasing compaction force.

Moreover, the results of ICR measurements obtained at the compaction pressure of 200 N cm^{-2} are shown in Fig. 9. It is evident that the interfacial contact resistance between the Al-alloy BPPs and GDLs increased with increasing precorroding (aging) time. The ICR values measured with the BPPs aged at the simulated cathode environments were higher than those on the anode side because of the thicker oxide film formed on the cathode BPPs. In summary, the cathode BPPs with oxide layers are more resistant to corrosion than the anode BPPs, but the surface conductivity of the cathode BPPs is inferior. The ICR results agree with the potentiodynamic polarization analyses and surface characterization on the aged BPPs.

4. Conclusions

A novel technique was proposed to investigate the degradation of metallic bipolar plates on PEMFC performance. This method created a simulated environment separated from the cell system to avoid interaction between the BPPs and the polymer membrane and exclude the degradation factor of membrane. Moreover, the novel method is different from conventional in situ and ex situ methods because it takes into account the mass transport effects and implements synchronous operation with a real cell. Therefore, the results examined in the simulated environment can be directly compared with those in real operation. Regardless of whether the Al-alloy BPPs were aged in real or simulated PEMFC environments, all performance polarization curves of the single cells assembled with these Al-alloy BPPs can be fitted well using the mathematical model. It can be confirmed that the BPP degradation tendency could be explored in much less time by adopting this method.

References

[1] S.Y. Lee, E.A. Cho, J.H. Lee, H.J. Kim, T.H. Lim, I.H. Hwan, J. Won, Journal of the Electrochemical Society 154 (2007) B194–B200.
[2] C.M. Lai, J.C. Lin, K.L. Hsueh, C.P. Hwang, K.C. Tsay, L.D. Tsai, Y.M. Peng, Journal of the Electrochemical Society 155 (2008) B843–B8510.
[3] R. Mukundan, J.R. DAvey, R.W. Lujan, J.S. Spendelow, Y.S. Kim, D.S. Hussey, D.L. Jacobson, M. Arif, L. Rodney, ECS Transactions 16 (2) (2008) 1939–1950.
[4] Y. Ishibashi, A. Nishikata, ECS Transactions 16 (24) (2009) 85–89.
[5] A.M. Abdullah, A.M. Mohammad, T. Okajima, F. Kitamura, T. Ohsaka, Journal of Power Sources 190 (2009) 264–270.
[6] Y. Hung, H. Tawfik, D. Mahajan, Journal of Power Sources 186 (2009) 123–127.
[7] C.Y. Bai, Y.H. Chou, C.L. Chao, S.J. Lee, M.D. Ger, Journal of Power Sources 183 (2008) 174–181.
[8] Y. Hung, K.M. El-Khatib, H. Tawfik, Journal of Power Sources 183 (2006) 509–513.
[9] S.A. Abo El-Enin, O.E. Abdel-Salam, H. El-Abd, A.M. Amin, Journal of Power Sources 177 (2007) 131–136.
[10] S.H. Wang, J. Peng, W.B. Lui, J.S. Zhang, Journal of Power Sources 162 (2006) 486–491.
[11] A. Oyarce, N. Holmström, A. Bodén, S. Randström, G. Lindbergh, ECS Transactions 25 (2009) 1791–1801.
[12] R.C. Makkus, A.H.H. Janssen, F.A. Bruijn, R.K.A.M. Mallant, Fuel Cells Bulletin 17 (2000) 5–9.
[13] D.R. Hodgson, B. May, P.L. Adock, D.P. Davies, Journal of Power Sources 96 (2001) 233–235.
[14] J. Wind, R. Spah, W. Kaiser, G. Bohm, Journal of Power Sources 105 (2002) 256–260.
[15] H. Wang, M.A. Sweikart, J.A. Turner, Journal of Power Sources 115 (2003) 243–251.
[16] A.M. Lafront, E. Ghali, A.T. Morales, Electrochimica Acta 52 (2007) 5076–5085.
[17] Y. Wang, D.O. Northwood, ECS Transactions 11 (18) (2008) 53–60.
[18] M.H. Oh, Y.S. Yoon, S.G. Park, Electrochimica Acta 50 (2004) 777–780.
[19] S.J. Lee, C.H. Huang, J.J. Lai, Y.P. Chen, Journal of Power Sources 131 (2004) 162–168.
[20] J. Kim, S.M. Lee, S. Srinivasan, Journal of the Electrochemical Society 142 (1995) 2670–2674.